2014 IEEE International Conference on Robotics & Automation (ICRA)
Hong Kong Convention and Exhibition Center
May 31 - June 7, 2014. Hong Kong, China

Powertrain Selection for a Biologically-Inspired Miniature Quadruped Robot

Onur Ozcan, Andrew T. Baisch, Daniel Ithier, and Robert J. Wood
Harvard University, School of Engineering and Applied Sciences, Cambridge, MA, USA

***Abstract*— Transmission and actuator selection are crucial for robot locomotion at any scale. This is especially true at small scales where actuation choices are limited and locomotion is energetically expensive. These components control the payload capacity and determine the height of the obstacles the robot can navigate over. In this study, we analyze the drivetrain of the new Harvard Ambulatory MicroRobot (HAMR-V) to improve its walking performance. We modeled several transmission and actuator design concepts and investigated their force and displacement outputs. The results led to the selection of improved actuator and transmission designs. Using these new insights, we constructed a miniature quadruped with a payload capacity of 63% of its weight that can be used for on-board electronics for sensing, control, and power.**

***Index Terms*— Biologically Inspired Robots, Legged Locomotion, Mobile Robotics, Miniature Robots.**

I. Introduction

The ability of some insects to robustly traverse rough terrain [1] and scale vertical and inverted surfaces [2] have motivated a variety of biologically-inspired terrestrial robots [3], [4], [5], [6], [7], [8]. These abilities make legged vehicles desirable for exploration of hazardous environments such as collapsed buildings or natural disaster sites. Our work focuses on the development of a sub-two gram walking platform capable of traversing rough terrain and eventually scaling vertical surfaces. In addition to providing accessibility to confined spaces, small robots will be more adept at climbing inclined and vertical surfaces due to surface area to volume scaling laws.

Previously, HAMR3, a 1.7 g, 4.7 cm long hexapod, demonstrated autonomous locomotion on flat ground up to 4.3 cm/s (0.9 body lengths per second) [9]. The design of HAMR3 focused on integrating on-board control and high-voltage power electronics while the mechanical powertrain, comprised of piezoelectric bending actuators and flexure-based transmissions, were not optimized. HAMR3, therefore, performed slower than desired, was unable to support a payload, and was incapable of traversing obstacles as small as 1 mm.

The experience acquired in the development of previous versions emphasized the importance of powertrain selection for such miniature legged platforms where payload capacity is limited. Actuator and transmission selection should focus on maximizing vertical leg displacement and force while minimizing mass and energy of the constituent components. Several designs avoid these problems by building the robot in the tens of grams mass range [10], [5], [4], [11] or larger [12], [13], allowing them to use DC or servo motors or even pneumatic actuators. In the sub-10 gram range, RoACH [3], uses light-weight shape memory alloy wires as the actuation mechanism. For our robot, piezoelectric bending actuators are used primarily due to their compatibility with the transmission fabrication process and high bandwidth.

The transmission and actuator selection for the robots mentioned above are discussed in literature. In addition, several models are suggested [14], [5], [11], [15] that explain transverse plane kinematics of a miniature legged robot. However, there is a lack of a comprehensive powertrain study focused on sagittal plane leg displacements and forces that would help researchers choose optimal design parameters to improve robots' payload capacities and rough terrain locomotion capabilities.

This work aims to improve HAMR's walking performance through the selection of a transmission and actuator design that satisfies requirements for a single leg's lift degree of freedom. In this paper, the development of a theoretical powertrain model is detailed. This model is used in combination with experimental results from a single robot leg system to choose actuator and transmission parameters that are implemented in our robot. Using these design parameters, a new biologically inspired quadruped, HAMR-V, is built and its payload capabilities are tested.

II. Problem Statement

A. Mechanical Design

HAMR-V has four legs, each with two degrees of freedom (DOF): lift and swing. Forward walking is achieved by appropriate phasing of these two DOFs and coupling contralaterally across the body. The two leg DOFs are achieved by using a flexure-based spherical five-bar linkage (SFB), previously described in HAMR2 [16] and utilized in both HAMR2 and HAMR3 [9]. The SFB linkage maps two actuator inputs to a 2 DOF leg motion: a swing DOF that provides locomotive power and a lift DOF that raises and lowers the leg in the sagittal plane. The inputs are decoupled and driven by two four-bar slider crank mechanisms actuated with piezoelectric bimorph cantilevers [17]. A drawing of this linkage is shown in Fig. 1(a).

The SFB is manufactured using the PC-MEMS fabrication paradigm [18], as described in [9]. A nine-layer linkage laminate consists of five functional material layers: a central polyimide (Kapton) flexure, two rigid three-ply [0, 90, 0] carbon fiber layers, and two outer brass bond pad layers. Acrylic sheet adhesive (DuPont FR) comprises the remaining four layers and bonds each subsequent functional layer. Each layer is first bulk micromachined using a UV diode-pumped-solid-state (DPSS) laser, resulting in the rigid links separated

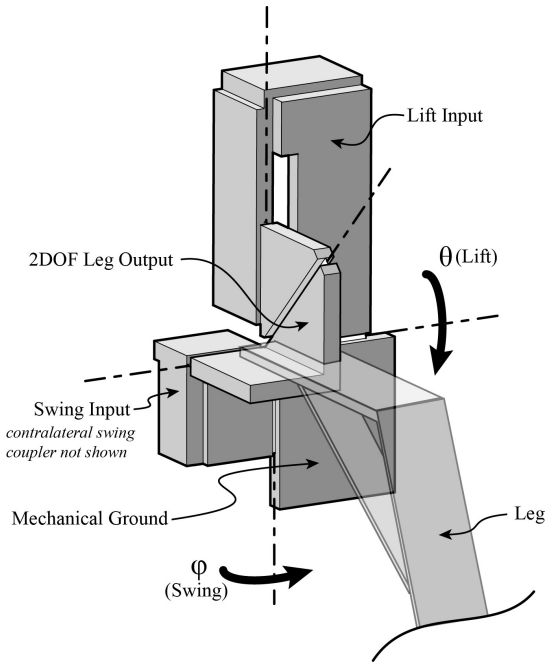

(a)

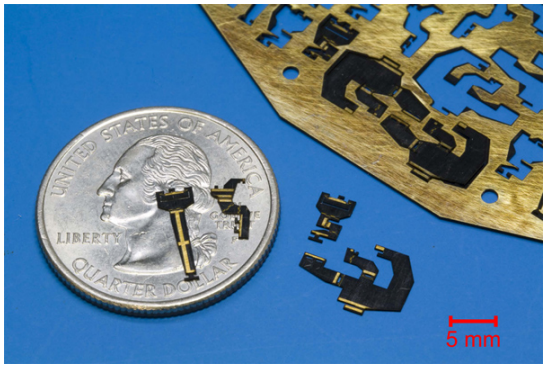

(b)

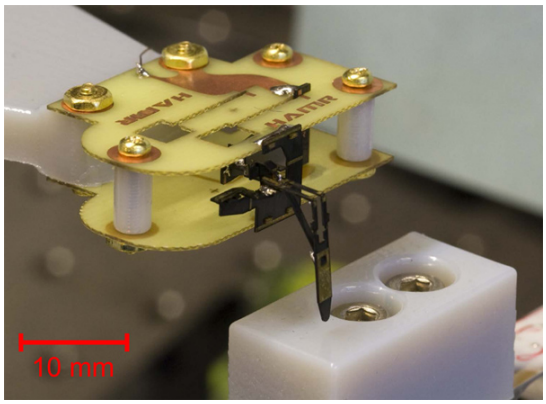

(c)

Fig. 1. (a) A drawing showing the flexure-based spherical five-bar hip joint utilized in all HAMR versions, which provides swing and lift outputs to the leg. (b) The fabricated planar parts of the transmission. (c) The assembled transmission, utilized in a single leg test setup. The top and bottom yellow plates are copper-clad FR4 and used for electrical connections and mechanical rigidity. The copper is etched to create electrical traces to power the actuators. The vertical carbon-fiber plate that connects the FR4 plates is the mechanical ground for the five-bar transmission.

by compliant flexures. The completed linkages are shown in Fig. 1(b).

The resulting links may be folded or mechanically interfaced with other parts to form 3D flexure-based mechanical linkages. Each "hip" joint is fabricated as four planar parts: two forming the two-DOF SFB, a swing slider-crank input, and a lift slider-crank input. Assembly of each joint requires two folds, followed by mating the four parts using built-in clip interfaces. As the last step, the parts are soldered at the brass pads to fix them in place. A picture of the completed transmission assembly is shown in Fig. 1(c).

Piezoelectric bimorph cantilevers, geometrically optimized for maximal energy density [17], are selected as actuators for the powertrain due to their simple geometries, scalability, and compatibility with the manufacturing methods used to create the transmission. These actuators have been used in HAMR2 [16] and HAMR3 [9] and other miniature robots [19], [18] and have sub-mm displacements (thus requiring amplification by the slider-crank mechanism), relatively high force production (100s of mN) and very high bandwidths. The actuators are composed of a central prepreg carbon fiber layer sandwiched by two 127 μm thick lead-zirconate-titanate (PZT-5H) plates and a patterned copper-clad FR-4 layer for electrical connections.

B. Lift Degree of Freedom Modeling

The criteria for HAMR's successful operation are three-fold: each leg should be able to statically support one-fourth of the body weight so that the body will not sag (see Fig. 2 for our definition of sagging) while standing with each actuator off; each leg should be able to carry half of the body weight during walking; and the leg displacement should be maximized in order to operate on rough terrain. Assuming the lift and swing DOFs are completely decoupled, a model of the lift DOF of the powertrain is developed to investigate the effects of various design parameters on locomotion. The model consists of the actuator as a force source in parallel with a spring, a serial compliance term, a kinematic model of the four-bar slider crank mechanism, and the compliances of three flexure joints of the four-bar slider crank. The serial compliance term compensates for the imperfections in fabrication, off-axis flexure compliance (e.g. flexure buckling) and compliance of the linkages or skeleton. An illustration of this model is shown in Fig. 3.

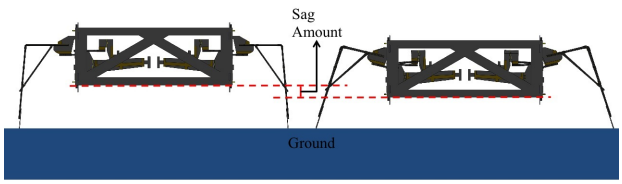

Fig. 2. A simplified drawing of two robots; the left exhibits no sagging problem whereas the right version can only carry its weight after preloading its transmission. The height difference between the bodies of these robots, i.e. the amount of vertical displacement the legs experience, is defined as the sag.

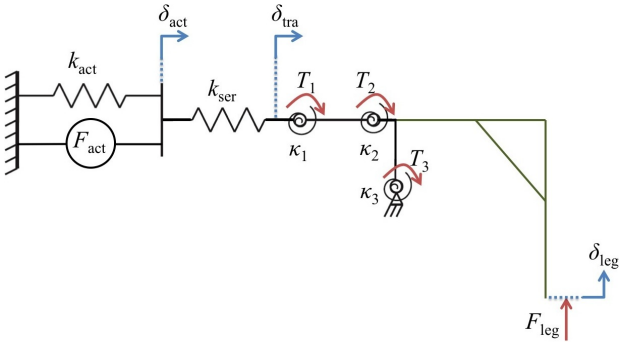

Fig. 3. A simplified drawing of the lift DOF actuation model which includes the actuator, serial compliance, and the four-bar slider crank mechanism.

Assuming all the stiffness values and linkage lengths are known, the system has a single degree of freedom. The displacement of the actuator can be directly mapped to the displacement of the leg. Writing a power balance yields:

$$F_{act}\frac{\partial\delta_{act}}{\partial t} - k_{act}\delta_{act}\frac{\partial\delta_{act}}{\partial t} + k_{ser}(\delta_{tra}-\delta_{act})\frac{\partial\delta_{act}}{\partial t}\cdots - k_{ser}(\delta_{tra}-\delta_{act})\frac{\partial\delta_{tra}}{\partial t} + \kappa_1\Phi_1\frac{\partial\Phi_1}{\partial t} + \kappa_2\phi_2\frac{\partial\Phi_2}{\partial t}\cdots + \kappa_3\Phi_3\frac{\partial\Phi_3}{\partial t} - F_{leg}\frac{\partial\delta_{leg}}{\partial t} = 0, \quad (1)$$

where F_{act} is the actuator force, δ_{act} is the actuator displacement, k_{act} is the actuator stiffness, k_{ser} is the serial compliance, δ_{tra} is the transmission displacement, and κ_i and Φ_i are the torsional compliances and rotation angles for the i^{th} four-bar joint, respectively. F_{leg} is the force experienced by the leg and δ_{leg} is the leg displacement. T_i's shown in fig. 3 are the resistance torques, and can be calculated as: $T_i = \kappa_i \times \Phi_i$. The transmission is assumed to be ideal (i.e. flexures act as ideal pins), which means that δ_{tra} can be directly mapped to δ_{leg}. Therefore, the following force balance equation holds:

$$F_{act} = k_{act}\delta_{act} = k_{ser}(\delta_{tra}-\delta_{act}), \quad (2)$$

which yields:

$$\frac{\partial\delta_{act}}{\partial\delta_{tra}} = \frac{1}{1+\frac{k_{act}}{k_{ser}}} = A. \quad (3)$$

The term A governs how much of the actuator deflection δ_{act} is lost due to imperfections and how much of it is conveyed on the transmission as δ_{tra}. As $k_{ser} \to 0$, i.e. the imperfections dominate the entire behavior of the powertrain, $A \to 0$, which means none of the actuator deflection will be conveyed on the transmission. On the other hand, as $k_{ser} \to \infty$, i.e. no imperfections, $A \to 1$, which means all of the actuator deflection will be conveyed on the transmission. Dividing eqn. (1) with $\partial\delta_{tra}/\partial t$ and substituting eqn. (3) in eqn. (1) yields:

$$AF_{act} - Ak_{act}\delta_{tra} + \kappa_1\Phi_1\frac{\partial\Phi_1}{\partial\delta_{tra}} + \kappa_2\phi_2\frac{\partial\Phi_2}{\partial\delta_{tra}}\cdots + \kappa_3\Phi_3\frac{\partial\Phi_3}{\partial\delta_{tra}} - F_{leg}R_{tra} = 0, \quad (4)$$

where $R_{tra} = \partial\delta_{leg}/\partial\delta_{tra}$ is the relative movement of the leg with respect to the movement of the transmission input; hence it is the instantaneous transmission ratio. The terms $\frac{\partial\Phi_1}{\partial\delta_{tra}}$, $\frac{\partial\Phi_2}{\partial\delta_{tra}}$, $\frac{\partial\Phi_3}{\partial\delta_{tra}}$, R_{tra} and δ_{tra} can be solved kinematically for a given leg displacement and the force experienced by the leg can be found if the stiffness values are known and the actuator force is either modeled or characterized experimentally.

C. Design Considerations

In order to increase the force experienced by the leg, the model in eqn. 4 suggests that one can change the joint stiffness values κ_1, κ_2, and κ_3, the actuator force F_{act} and stiffness k_{act}, and the transmission ratio R_{tra} (assuming serial compliance cannot be controlled). The stiffness of the joint can be modified by changing either the flexure geometry or the polyimide layer thickness. Actuator force and stiffness can be controlled by changing actuator geometry or the central carbon fiber layer thickness. The transmission ratio can be chosen either by changing any of the transmission link lengths or the length of the link that connects the transmission to the actuator, i.e. the input link length. For this study, we chose to change the polyimide layer thickness (the blue layer in Fig. 4) to control joint stiffness values, since it does not require a redesign of the joints. In a similar fashion, to control the transmission ratio, we chose to change the input link length of the transmission (the red linkage in Fig. 4) which does not require the rest of the robot body to be redesigned. Changing the input link length without changing the actuator and 'hip' joint positions changes the neutral position of the transmission and stores energy in the actuator and transmission springs. As a result, a position and force bias is added to the transmission opposing gravity. Therefore, the transmission ratio is effectively changed without redesigning any other transmission parts. To control the actuator force output and stiffness, we chose to change the central carbon fiber layer thickness (the green layer in Fig. 4) since this would have negligible impact on the design of other body components. To prevent HAMR-V from sagging during its operation, the required actuator force, and thus drive voltage, must also be found. Ideally these designs would only minimally reduce free displacement. In addition, the effect of adding the swing DOF should be investigated to see if there are any issues with the coupling between lift and swing DOFs.

III. Experimental Setup

An experimental setup to test the completed transmissions is built from a vertical motorized positioning stage, a single-axis force sensor, drive electronics and a camera. The force sensor (RSP2, Loadstar Sensors) is attached on a three-axis manual positioner (Newport). The transmission with a leg and an actuator is attached to a motorized stage (UTS100PP, Newport) controlled through its dedicated controller (SMC100PP, Newport). The motorized stage controller is commanded from a PC through Matlab xPC, which also reads the sensor output and runs the actuator attached

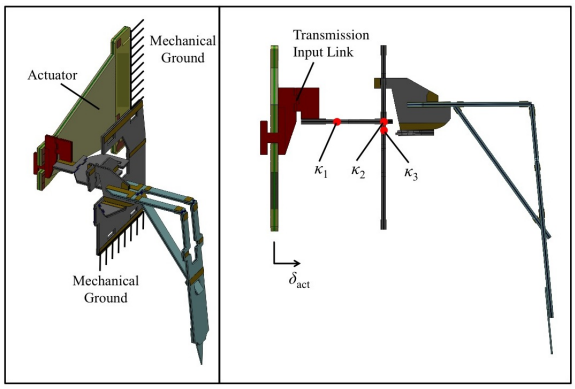

(a)

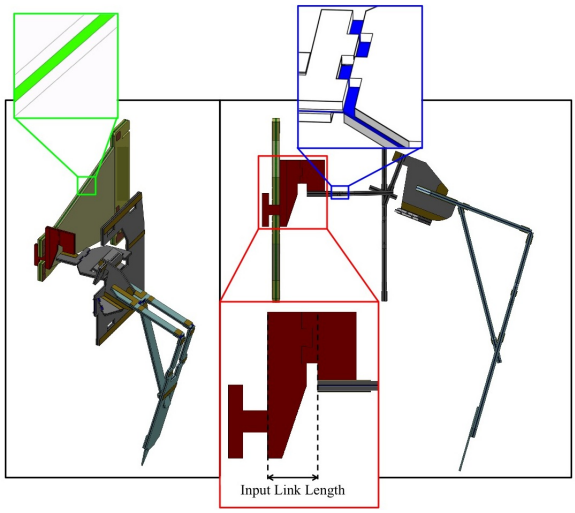

(b)

Fig. 4. (a) Solidworks rendering of a nominal powertrain. The red component is the input linkage to the transmission whose length controls the transmission bias (shown in detail in bottom inset in (b)). The blue layer that can be seen at the joints is the polyimide layer (Kapton) whose thickness alters the joint stiffness values (shown in detail in top-right inset in (b)). The green layer at the actuator center is the carbon fiber layer whose thickness controls the actuator stiffness and force output (shown in detail in the top-left inset in (b)). (b) Solidworks rendering of a biased powertrain. Extending the length of the input linkage causes compression in the transmission; the transmission links on each side of joint 1 bend downwards (joint 1 becomes concave) while links on each side of joint 2 bend upwards (joint 2 becomes convex) and the lift hip link (the movable link between joint 2 and 3) bends down. These deflections move the neutral position of the leg down, providing a bias to the transmission and effectively changing the transmission ratio.

to the transmission using a DAQ board (Measurement Computing, PCI-DAC6703) and custom high voltage amplifiers. A picture showing the transmission test setup is shown in Fig. 5(a).

In order to characterize the actuators with different carbon fiber thicknesses, an experimental setup involving manual positioning stages (Newport), a six-axis force/torque sensor, actuator drive electronics, and a camera is used. The actuators are clipped to the drive electronics that includes a DAQ board (National Instruments, NI PCI-6052E) controlled via Matlab xPC and high voltage amplifiers (TREK, PZD350A). The actuators are then brought into contact with the force sensor (ATI Industrial Automation, Nano 17) with no load

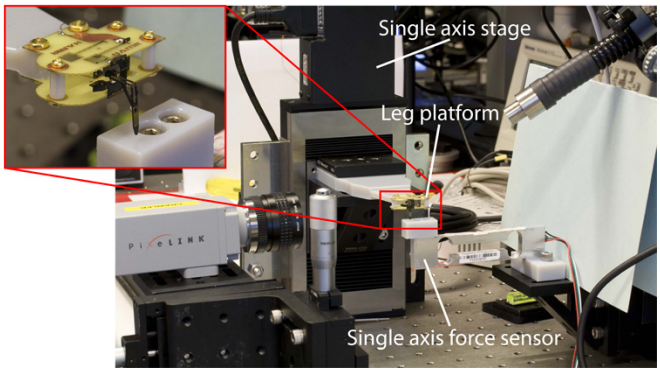

(a)

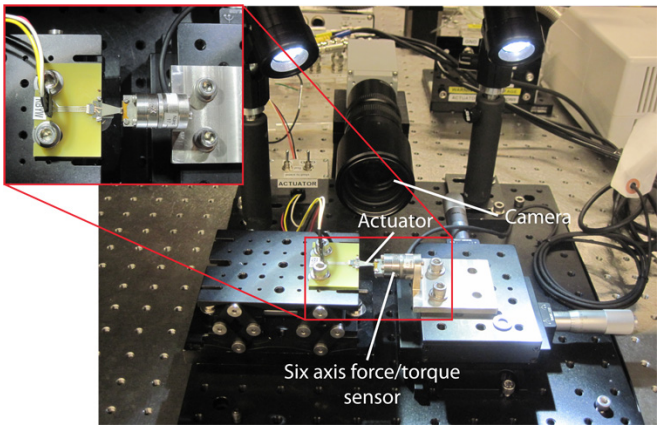

(b)

Fig. 5. Experimental setups: (a) Transmission test setup and (b) actuator test setup.

applied. The actuators are driven with varying drive voltages and the resulting force data is collected by the force sensor and displacement is recorded using a camera (PixeLINK, PL-B741F). This test setup is shown in Fig. 5(b).

IV. Actuator Selection

The first component that should be addressed in optimizing the HAMR's powertrain is actuator selection. The actuator must be able to provide sufficient force to enable the robot to carry its weight while simultaneously maximizing displacement. The actuators should also have a high energy density so that their contribution to the robot mass will be minimal. As discussed in section II, optimal energy density piezoelectric bimorph cantilevers are selected for our robot. Three different actuators are built with one (1x in Fig. 7), two (2x in Fig. 7), and three (3x in Fig. 7) central carbon fiber layers. Central layer thickness is chosen so that we can explore the tradeoff between force and displacement (a thicker central layer increases blocked force at the expense of displacement) without altering the planar geometry. All the other design parameters are kept constant and their reported (or designed for geometric parameters) values are given in Table I. The definitions of these parameters can be found in [17].

Actuator force and displacement are calculated using the laminate plate model in [17]. The actuators are also tested using the actuator test setup described in section III. The

TABLE I

ACTUATOR PARAMETERS

Parameter	Reported	Effective
Carbon Fiber Thickness (μm)	60 (Uncured)	30 (Cured)
PZT Plate Thickness* (μm)	127	155
FR4 Layer Thickness (μm)	127	127
Actuator Length* (mm)	8.8	9.6
Actuator Nominal Width* (mm)	4.2	3.4
Actuator Length Ratio	0.0063	0.0063
Actuator Width Ratio	1.5	1.5
PZT d31 Strain Coefficient* (nm/V)	0.35	0.36
PZT Young's modulus* (GPa)	42	34

Note: The effective values of the parameters marked with * are found by fitting the model to the experiments.

actuators are driven with a trapezoid signal between the ground and bias voltage; a square signal would maximize time-averaged force/displacement however a ramp decreases the likelihood of damaging actuators by exciting the actuator resonance. The voltages listed in Fig. 7 are the bias voltage values. The actuator has maximum deflection when the drive voltage is equal to the ground or the bias voltage, and has no deflection where the drive voltage is half of the bias (see Fig. 6).

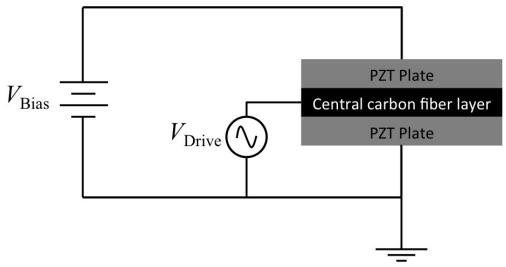

Fig. 6. A side view schematic of the optimal density energy piezoelectric bimorph cantilever. V_{Bias} is the bias voltage, connected to the top PZT plate, V_{Drive} is the drive voltage, connected to the central carbon fiber layer, and the bottom PZT plate is grounded. When $V_{\text{Drive}} = V_{\text{Bias}}$, the actuator bends up; when $V_{\text{Drive}} = 0$, the actuator bends down; when $V_{\text{Drive}} = V_{\text{Bias}}/2$, the actuator is neutral.

The instantaneous force and displacement during a step cycle are recorded. The half cycle energy, defined as the product of blocked force and free displacement, of the actuator for a given drive voltage is found using the force and displacement data and this energy is divided by the actuator's mass to acquire the energy density for a given actuator. The result of the experiments and the simulations are shown in Fig. 7. The simulations are run using the third column of Table I which are the effective values of actuator parameters. These values are found by fitting the simulation results to experiment results using the Nelder-Mead method [20]. The parameters that are found by fitting are the Young's modulus of PZT, PZT d_{31} strain coefficient, PZT plate thickness, actuator length, and actuator nominal width values. These parameters are chosen since they have the largest impact on actuator performance and are also most easily affected by actuator fabrication and handling methods. The Young's modulus of PZT and the effective width of the actuator are found to be lower than reported, which may be the result of field-dependent effects on the modulus and reduced effective width due to laser cutting, respectively. By direct measurement, we found that the PZT plates are often thicker than the reported 127 μm, which is reflected in our fits. We also found the effective length to be greater due to imperfect mechanical grounding of the actuators, resulting in small displacements at the base, effectively increasing tip displacement.

The agreement between the model with fitted parameters and the experiment results are acceptable for design purposes. Even though the actuator with a single carbon fiber layer is optimal for displacement and the actuator with three carbon fiber layers has the largest force output, the actuator with two central carbon fiber layers has the highest energy density. Therefore, actuators with two central carbon fiber layers are chosen to drive the new transmission of our robot.

V. TRANSMISSION SELECTION

As discussed in section II-B, the powertrain must be able to apply a force equal to half the body weight during walking, one-fourth of body weight during standing, and also achieve a large displacement to overcome obstacles. In order to test these cases, we constructed four different designs by changing the two parameters described in section II: the bias of the transmission and the polyimide layer (Kapton) thickness. A fifth transmission is also built, by adding the swing DOF to the fourth design, to test if the addition of the second DOF to the transmission would change its force and displacement characteristics. The parameters for these designs are shown in Table II. The values of these parameters are chosen for practical reasons: the Kapton thicknesses of 12.5 μm and 25 μm are commercially available and the 200 μm bias is chosen to match the average deflection that the actuators experience at 250 V, i.e. the neutral position of the foot for the biased transmission is the same as the lowest vertical position of the foot that the baseline transmission reaches.

TABLE II

TRANSMISSION DESIGNS

Design	Kapton Thickness (μm)	Bias Length (μm)	DOFs
1	12.5	0	Only Lift
2	25	0	Only Lift
3	12.5	200	Only Lift
4	25	200	Only Lift
5	25	200	Lift and Swing

Note: The designs 1-5 are referred in the text as: "baseline", "double thick Kapton", "biased", "biased with double thick Kapton", and "biased with double thick Kapton – 2 DOF", respectively.

Experimental blocked force data with zero sag (where the neutral position of the leg is barely touching the force sensor) and at different sag amounts (where the leg position is offset a prescribed sag amount from the surface of the force sensor) are taken using the experimental setup described in section III. For the zero sag experiments, drive voltages are varied from 100 V to 250 V in 50 V increments. The upper limit of 250 V is chosen to avoid mechanical failure of the piezoelectric ceramics. A drive voltage of 250 V is used for varying sag experiments, where the sag amount is varied from 0 to 3 mm in 1 mm increments. The resulting data is shown in Fig. 8.

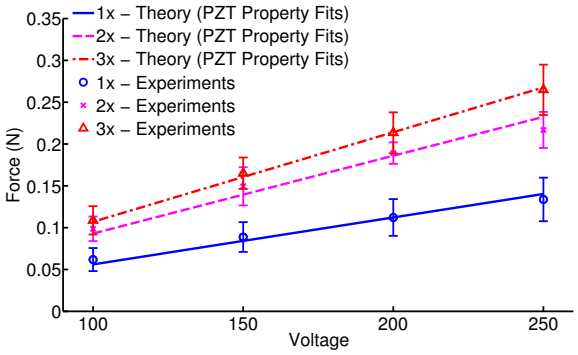

(a)

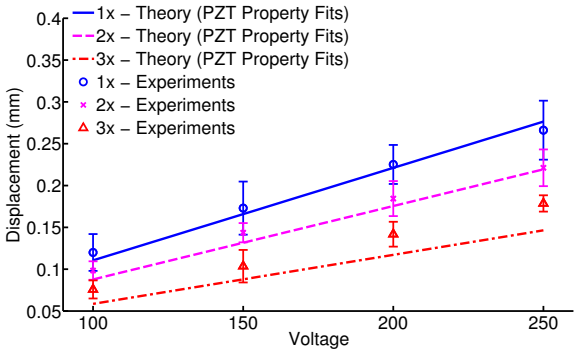

(b)

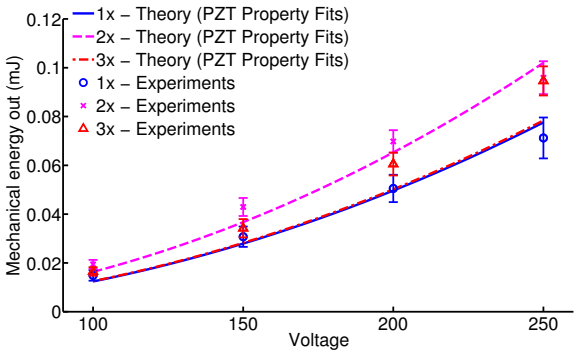

(c)

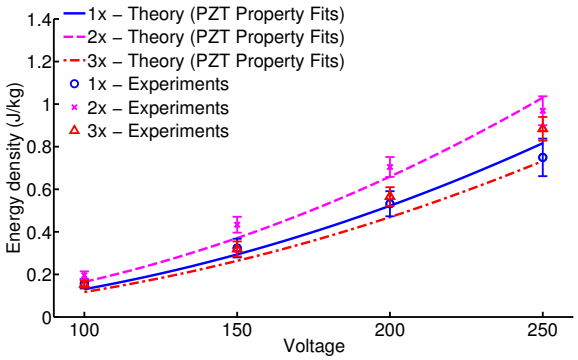

(d)

Fig. 7. Simulation and experimental results of actuators with varying carbon fiber layer thickness. The solid lines are theoretical results and the data points with error bars are experimental data. Each error bar is the standard deviation of 25 data points acquired from 3 actuators. (a) Actuator force, (b) Actuator displacement, (c) Actuator energy, and (d) Actuator energy density.

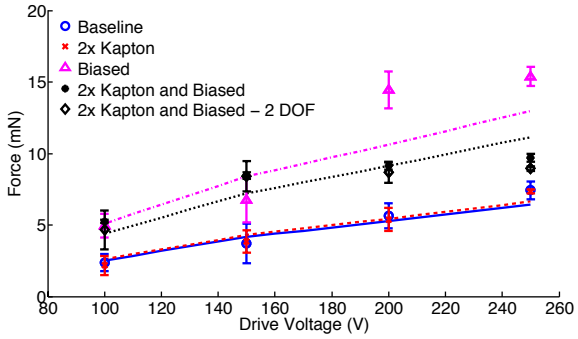

(a)

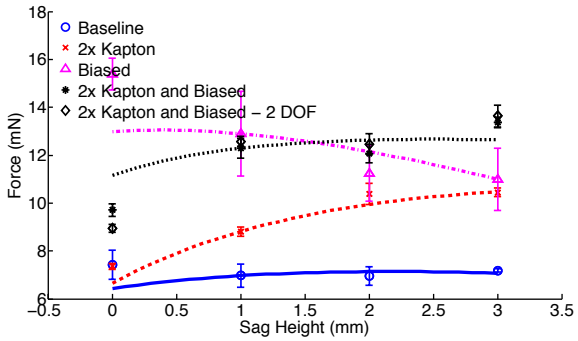

(b)

Fig. 8. Blocked force experiments and simulations of different designs. The solid lines are theoretical results and the data points with error bars are experimental data. The error bars represent the standard deviation of five experiments. (a) Force experienced by the leg without any body sag. (b) Force experienced by the leg at different sag heights at 250 V drive.

The model described in section II is fitted to these data points in order to find the serial compliance arising from undesired compliance of the body and transmission and fabrication errors. The joint stiffness values can be found using the pseudo rigid body approximation; however such modeling is sensitive to geometry. Therefore, the joint stiffness values are also found by fitting to account for fabrication errors. In addition to these parameters, the actual bias amount experienced by the transmission is also found by this fit since the prescribed bias amount (200 μm) is also affected by fabrication and assembly imperfections. A simple cost function of RMS error between the data and simulation is used and this error is minimized using Nelder-Mead method to find the missing parameter values. The values found by this fit are shown in table III and the simulation results using the fitted values are shown in Fig. 8. As expected, the fitted parameter values suggest that the joint stiffness values increase with increased Kapton thickness, and the bias values are close to the designed values.

HAMR-V weighs 10.6 mN, hence the transmissions should be able to generate 5.3 mN of force during walking. As can be seen from Fig. 8(a), without sagging, the "baseline" and "double thick Kapton" designs cannot generate enough force below 250 V, whereas, the other three designs can generate enough force for walking at drive voltages above 150 V. On the other hand, all transmissions can generate enough force for walking once they sag (Fig. 8(b)).

TABLE III

FITTED PARAMETER VALUES

Param.	Baseline	Biased	Double Thick Kapton	Biased With Double Thick Kapton
k_{ser}	800	2600	810	850
κ_1	$< 10^{-6}$	$< 10^{-6}$	0.019	0.023
κ_2	$2.41 \cdot 10^{-5}$	$< 10^{-6}$	$5.93 \cdot 10^{-5}$	$8.21 \cdot 10^{-5}$
κ_3	$< 10^{-6}$	$< 10^{-6}$	$8.11 \cdot 10^{-5}$	$< 10^{-6}$
Bias	-10	146	-19	183

Note: The units of k_{ser}, κ values and Bias are N/m, Nm/rad, and μm, respectively.

The free displacement of the legs is also recorded and compared with the simulations using fitted parameters, as can be seen in Fig. 9. Both simulations and the experimental data show that the "biased with double thick Kapton" transmission design, which is expected to be the stiffest transmission, has the lowest displacement output whereas the baseline design, which is the softest, has the highest displacement.

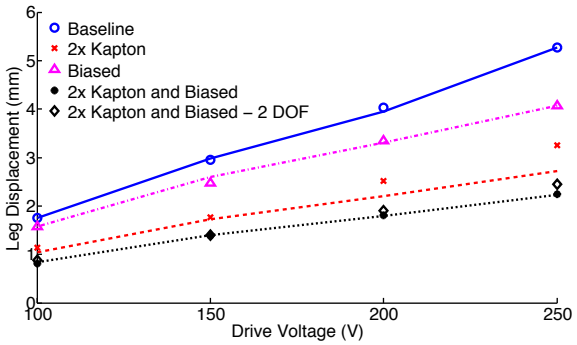

Fig. 9. Free displacement experiments and simulations of different designs. As expected, baseline design has the highest displacement whereas the "biased with double thick Kapton" has the lowest.

The stiffening of the robot's transmission causes us to sacrifice free leg displacement, however the actual vertical leg displacement experienced during walking is the difference between sag amount and the free displacement. Therefore, a transmission that is not sagging is also desirable to increase vertical leg displacement.

Among these candidates the "biased with double thick Kapton" design is chosen as the ideal transmission candidate because its force output is high enough for walking without sagging (see Fig. 8(a)) and the force output continues to increase as the sag amount increases (see Fig. 8(b)), which means it has the highest probability of carrying the greatest payload. "Biased" design is considered a close second, but is not chosen due to the decrease of its force output as the robot sags (see Fig. 8(b)), which implies that it would be harder for HAMR to recover if it sags for any reason (increased payload or uneven terrain).

We have also investigated the effect of adding the swing DOF to the transmission on the force output. A "biased with double thick Kapton" transmission with both lift and swing degrees of freedom is built and the same experiments are repeated. As can be seen from figures 8 and 9, the addition of the second DOF causes negligible change.

Besides the walking case, the static case should also be investigated. We have used our model to simulate the force response of the transmissions for different leg displacements where the actuator is not driven. The results of these simulations are shown in Fig. 10. The simulations suggest that for the "biased with double thick Kapton" design, the leg should displace 0.5 mm in order to support one-fourth of the HAMR's weight, i.e. it will sag 0.5 mm in static case. This sag amount would increase to 2 mm for "baseline" design.

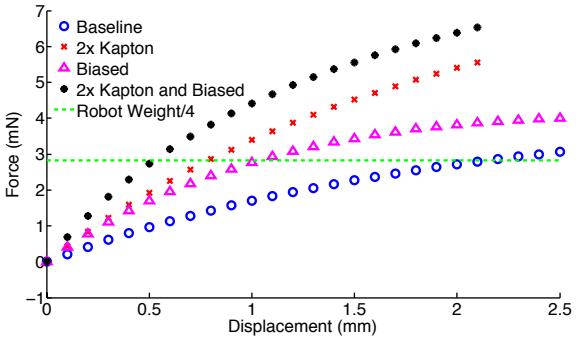

Fig. 10. Force-displacement simulations of different designs using the fitted stiffness and bias values. The dashed line shows one-fourth of the robot's weight, which should be carried by the legs at static position.

VI. FULL BODY EXPERIMENTS

A new version of HAMR, HAMR-V, is built using the optimal actuator and transmission identified in sections IV and V. A picture of the robot is shown in Fig. 11. The new version is a quadruped, driven with optimal energy density piezoelectric biomorph cantilever type actuators with two central carbon fiber layers. These actuators are attached to a five-bar transmission with double thick Kapton joints (25 μm thickness) and a 200 μm-bias. The four sides of the robot body are made of laser-machined [0, 90, 0] precured carbon fiber composite and the top and bottom plates are copper-clad FR4. The copper on FR4 is etched to create electrical traces required to run the actuators. The current version is tethered and driven with a Matlab script running on a PC connected to an xPC target to generate the drive signals. Its mass is 1.08 g, making it one of the lightest robots capable of legged locomotion.

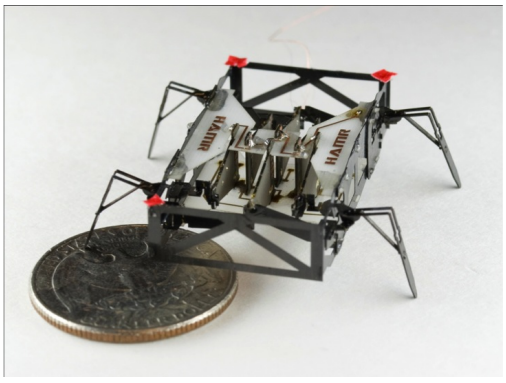

Fig. 11. The new quadruped built with the optimal powertrain described in sec. V.

In order to test the payload capacity of HAMR-V, we add weights to the robot and run it at different drive frequencies

while recording its walking speed. The robot does not have on-board electronics and the Matlab script currently does not implement any closed-loop control. The results of the payload tests are shown in Fig. 12.

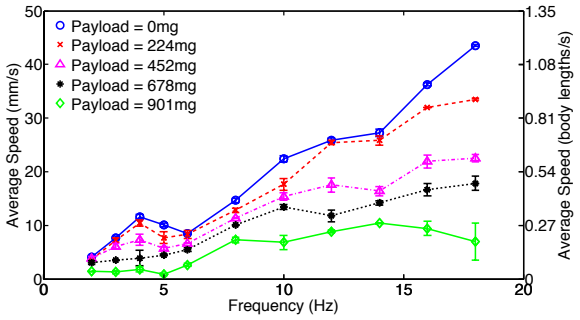

Fig. 12. Speed vs. frequency data of the quadruped without any payload and under four different payloads. As expected, the increase in payload slows the robot down and the robot walks faster as the drive frequency increases.

The results shown in Fig. 12 suggest a 678 mg maximum payload capacity for the robot. Even though HAMR-V carrying 901 mg can move at high frequencies, the observed motion is more similar to vibrating than walking and does not have a preferential direction. Hence, the payload capacity of robot is 678 mg, which is 63% of the robot's mass.

VII. Conclusion

Transmission and actuator selection of HAMR-V, a bioinspired quadruped, is described in this work. The actuator and the transmission are modeled using kinematic and power balance equations. Four transmission designs and three actuator designs are presented and improved actuator and transmission designs for the robot are identified. These new designs are used to build HAMR-V which can carry an additional mass of 678 mg. The addition of swing degree of freedom is shown to not effect the force output of the powertrain. Although the required force and displacement outputs change from robot to robot, we believe the model and the analysis described in this work can be used for similar robots that are fabricated using PC-MEMS manufacturing techniques.

Following this work, locomotion studies on the robot will be conducted and a fully autonomous version of this robot will be built using power and control electronics similar to [9]. A camera, an inertial measurement unit (IMU), and other sensors will be integrated to control locomotion. Compliant leg designs for increased robustness and foot attachment mechanisms for potential climbing applications will also be investigated.

Acknowledgments

The authors would like to thank all Harvard Microrobotics Laboratory group members for their invaluable discussions. This work is partially funded by the Wyss Institute for Biologically Inspired Engineering and the Army Research Labs Micro Autonomous Systems and Technology Program.

References

[1] S. Sponberg and R. Full, "Neuromechanical response of musculoskeletal structures in cockroaches during rapid running on rough terrain," *Journal of Experimental Biology*, vol. 211, pp. 433 – 446, May 2008.

[2] D. Goldman, T. Chen, and D. Dudek, "Dynamics of rapid vertical climbing in cockroaches reveals a template," *Journal of Experimental Biology*, vol. 209, no. 15, pp. 2990 – 3000, 2006.

[3] A. Hoover, E. Steltz, and R. Fearing, "Roach: An autonomous 2.4g crawling hexapod robot," in *Intelligent Robots and Systems, 2008. IROS 2008. IEEE/RSJ International Conference on*, sept. 2008, pp. 26 – 33.

[4] A. Hoover, S. Burden, X.-Y. Fu, S. Sastry, and R. Fearing, "Bio-inspired design and dynamic maneuverability of a minimally actuated six-legged robot," in *Biomedical Robotics and Biomechatronics (BioRob), 2010 3rd IEEE RAS and EMBS International Conference on*, sept. 2010, pp. 869 – 876.

[5] P. Birkmeyer, K. Peterson, and R. Fearing, "Dash: A dynamic 16g hexapedal robot," in *Intelligent Robots and Systems, 2009. IROS 2009. IEEE/RSJ International Conference on*, oct. 2009, pp. 2683 – 2689.

[6] S. Kim, M. Spenko, S. Trujillo, D. Santos, and M. Cutkosky, "Smooth vertical surface climbing with directional adhesion," *IEEE Transactions on Robotics*, vol. 24, pp. 65 – 74, Feb. 2008.

[7] S. Kim, A. Asbeck, M. Cutkosky, and W. Provancher, "Spinybot II: climbing hard walls with compliant microspines," in *Advanced Robotics, 2005. ICAR '05. Proceedings., 12th International Conference on*, july 2005, pp. 601 – 606.

[8] M. Murphy, C. Kute, Y. Menguc, and M. Sitti, "Waalbot II: Adhesion recovery and improved performance of a climbing robot using fibrillar adhesives," *The Internation Journal of Robotics Research*, vol. 30, no. 1, pp. 118 – 133, 2011.

[9] A. T. Baisch, C. Heimlich, M. Karpelson, and R. J. Wood, "HAMR^3: An autonomous 1.7g ambulatory robot," in *Intelligent Robots and Systems (IROS), 2011 IEEE/RSJ International Conference on*, sept. 2011, pp. 5073 – 5079.

[10] A. Pullin, N. Kohut, D. Zarrouk, and R. Fearing, "Dynamic turning of 13 cm robot comparing tail and differential drive," in *Robotics and Automation (ICRA), 2012 IEEE International Conference on*, may 2012, pp. 5086 –5093.

[11] K. Peterson and R. S. Fearing, "Experimental dynamics of wing assisted running for a bipedal ornithopter," in *Intelligent Robots and Systems (IROS), 2011 IEEE/RSJ International Conference on*, sept. 2011, pp. 5080 –5086.

[12] G. Nelson, R. Quinn, R. Bachmann, W. Flannigan, R. Ritzmann, and J. Watson, "Design and simulation of a cockroach-like hexapod robot," in *Robotics and Automation, 1997. Proceedings., 1997 IEEE International Conference on*, vol. 2, apr 1997, pp. 1106 –1111 vol.2.

[13] J. Clark, J. Cham, S. Bailey, E. Froehlich, P. Nahata, R. Full, and M. Cutkosky, "Biomimetic design and fabrication of a hexapedal running robot," in *Robotics and Automation, 2001. Proceedings 2001 ICRA. IEEE International Conference on*, vol. 4, 2001, pp. 3643 – 3649 vol.4.

[14] Y. Gao, W.-h. Chen, and Z. Lu, "Kinematics analysis and experiment of a cockroach-like robot," *Journal of Shanghai Jiaotong University (Science)*, vol. 16, pp. 71–77, 2011.

[15] K. Karydis, I. Poulakakis, and H. G. Tanner, "A switching kinematic model for an octapedal robot," in *Intelligent Robots and Systems (IROS), 2012 IEEE/RSJ International Conference on*, oct. 2012, pp. 507 –512.

[16] A. Baisch, P. Sreetharan, and R. Wood, "Biologically-inspired locomotion of a 2g hexapod robot," in *Intelligent Robots and Systems (IROS), 2010 IEEE/RSJ International Conference on*, oct. 2010, pp. 5360 – 5365.

[17] R. Wood, E. Steltz, and R. Fearing, "Optimal energy density piezoelectric bending actuators," *Sensors and Actuators A: Physical*, vol. 119, no. 2, pp. 476 – 488, 2005.

[18] P. Sreetharan, J. Whitney, M. Strauss, and R. Wood, "Monolithic fabrication of millimeter-scale machines," *Journal of Micromechanics and Microengineering*, vol. 22, no. 5, p. 055027, 2012.

[19] K. Hoffman and R. Wood, "Passive undulatory gaits enhance walking in a myriapod millirobot," in *Intelligent Robots and Systems (IROS), 2011 IEEE/RSJ International Conference on*, sept. 2011, pp. 1479 – 1486.

[20] J. A. Nelder and R. Mead, "A simplex method for function minimization," *The computer journal*, vol. 7, no. 4, pp. 308–313, 1965.